Available online at www.sciencedirect.com

ScienceDirect

Biochimica et Biophysica Acta 1758 (2006) 868–873

BIOCHIMICA ET BIOPHYSICA ACTA

BBA

www.elsevier.com/locate/bbamem

Is photobleaching necessary for Raman imaging of bone tissue using a green laser?

Kurtulus Golcuk [a], Gurjit S. Mandair [a], Andrew F. Callender [a], Nadder Sahar [b], David H. Kohn [b,c], Michael D. Morris [a,*]

[a] Department of Chemistry, University of Michigan, Ann Arbor, MI 48109, USA
[b] Department of Biologic and Materials Sciences, University of Michigan, Ann Arbor, MI 48109, USA
[c] Department of Biomedical Engineering, University of Michigan, Ann Arbor, MI 48109, USA

Received 13 January 2006; received in revised form 14 February 2006; accepted 16 February 2006
Available online 15 March 2006

Abstract

Raman microspectroscopy is widely used for musculoskeletal tissues studies. But the fluorescence background obscures prominent Raman bands of mineral and matrix components of bone tissue. A 532-nm laser irradiation has been used efficiently to remove the fluorescence background from Raman spectra of cortical bone. Photochemical bleaching reduces over 80% of the fluorescence background after 2 h and is found to be nondestructive within 40 min. The use of electron multiplying couple charge detector (EMCCD) enables to acquire Raman spectra of bone tissues within 1–5 s range and to obtain Raman images less than in 10 min.

Keywords: Raman microspectroscopy; Raman imaging; Photobleaching; Bone; EMCCD

1. Introduction

The mechanical properties of whole cortical bone are determined by its mass, geometry, and intrinsic composition [1]. However, these parameters alone cannot fully explain the variance in the mechanical properties of bone at the microstructural level [2–4]. At this level, cortical bone is comprised of interstitial lamellae and secondary osteonic lamellae microarchitectures, which are known to exhibit different mechanical properties. Such anisotropic mechanical properties have been linked to the difference in the hierarchical organization and orientation of the mineralized collagen fibers, as well as the history of the bone (e.g., diet, maturity, disease state, and the degree of microdamage) [5–7]. It is therefore necessary to establish an accurate and thorough understanding of these microstructural organizations in isolation and in relation to the biomechanical properties of bone.

Our group has previously shown that Raman microspectroscopy and Raman imaging are invaluable tools for the study of bone tissue. We have examined biomechanical properties [8–12] and in vitro mineralization process [13]. Raman spectroscopy is advantageous for its high information content and micron-range spatial resolution. Using multivariate curve resolution techniques, small variations in local composition can be detected and imaged [8–10].

While Raman spectroscopy is a useful imaging method, it suffers from two major limitations. Because the tissue is fluorescent, Raman spectroscopy and imaging are frequently performed with a near-infrared (NIR) laser, such as a 785 nm diode laser, which excites little bone fluorescence. Compared to the green (532 nm) lasers widely used in Raman spectroscopy, the use of a 785-nm diode laser results in long acquisition times. We routinely collect a line of 128 or 256 spectra in 30 s to 3 min using a line focused 785 nm laser. The long acquisition time is a result of the inverse-fourth power dependence of Raman intensity with excitation wavelength and the low quantum efficiency of CCD detectors at wavelengths above about 800 nm. At 785 nm, Raman scattering is about five times less intense than at 532 nm and the quantum efficiency of a deep depletion back-illuminated CCD–the best available detector for the 800–900 nm range in

* Corresponding author. Tel.: +1 734 764 7560; fax: +1 734 649 1179.
E-mail address: mdmorris@umich.edu (M.D. Morris).

0005-2736/$ - see front matter © 2006 Elsevier B.V. All rights reserved.
doi:10.1016/j.bbamem.2006.02.022

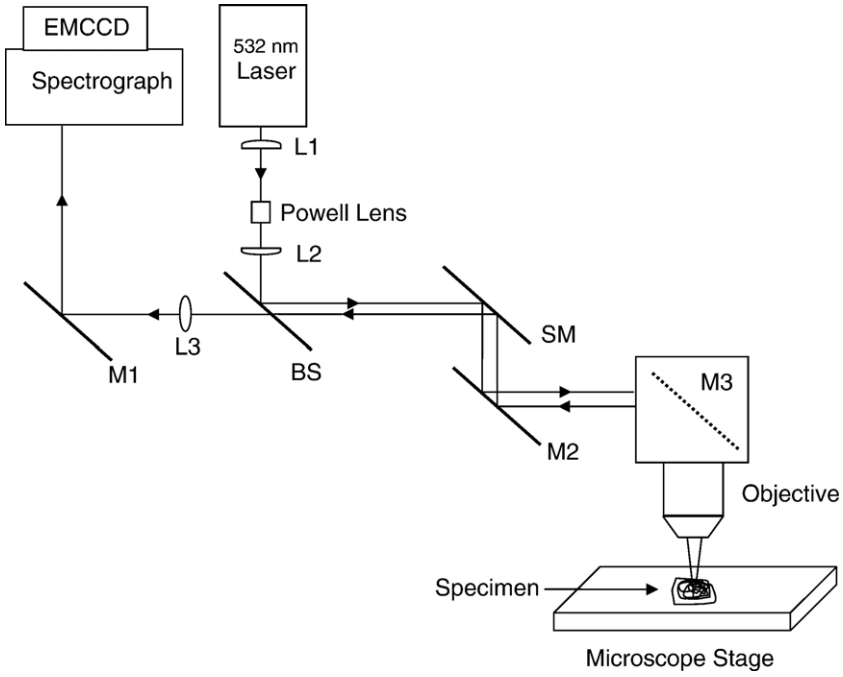

Fig. 1. Schematic representation of line scanning Raman microscope (LSRM). L1, L2, and L3: positive lenses; SM: scanning mirror; BS: beam splitter; M1, M2, and M3: mirrors; EMCCD: Electron Multiplying CCD.

which 785 nm excited bone mineral spectra and matrix amide I and amide III spectra are found–is about 30–40% [14]. By contrast, a back-illuminated CCD operating in the 550–600 nm range has quantum efficiency about 80–90%.

In addition, bone scatters light. Since the pioneering work of Matousek et al. [15] using time-resolved Raman spectroscopy, the effects of multiple scattering on Raman spectra have been intensively investigated [16,17]. It is known that as light propagates through a scattering medium such as bone [18–20], the light beam spreads out, resulting in Raman occurring at sites removed from the initial direction of laser beam entry into the tissue. The Raman scattered light itself undergoes multiple scattering. The overall effect can be modeled by a random walk. The multiple scattering effects are now generally called Raman photon migration [21], by analogy to multiple scattering effects in absorption and fluorescence

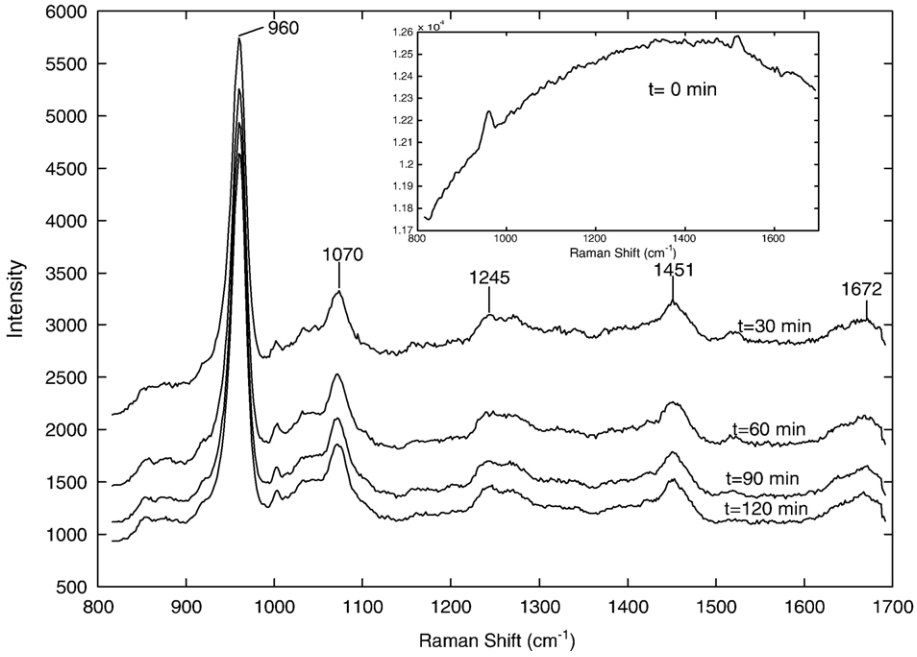

Fig. 2. Representative Raman spectra of bovine bone at different photobleaching time. Laser power is set to 150 mW.

spectroscopy. Photons that undergo multiple scattering are called diffusive photons.

The recently developed electron-multiplied CCD (EMCCD) [22] provides low noise gain and has the potential for reducing Raman spectral acquisition times a factor of 10–40. The back-illuminated EMCCD has already been applied to low-light level fluorescence imaging applications, including ultra-sensitive detection of intracellular calcium concentrations [22], optical tracking of single proteins [23] and imaging of tumor-targeted molecular probes [24].

However, to fully exploit the sensitivity of the back-illuminated EMCCD for 532 nm laser Raman imaging of bone, it is necessary to reduce the fluorescence background, which otherwise obscures the Raman spectrum of musculoskeletal tissues. Two general approaches have been proposed to minimize bone tissue fluorescence: chemical bleaching with 30% hydrogen peroxide [25] and photochemical bleaching with a 532 nm laser [26]. The chemical procedure has the disadvantage that there is an only very short time between the destruction of fluorescent impurities and damage to the tissue itself [27]. While no drawbacks were reported for the photochemical procedure, the 4-h treatment times were excessively long. In this study, we examine modified photochemical bleaching protocols that enable fluorescence reduction within 20 min, depending on the specimen. As we demonstrate, Raman photon migration effects the bleaching time and can be used to shorten the overall measurement time.

2. Materials and methods

The hyperspectral Raman imaging system (Fig. 1) is similar to our earlier design [28], except that a scanning stage that translates the specimen under a fixed laser line has been replaced by a galvanometer scanning mirror that sweeps the laser line across a stationary specimen. It consists of a research grade microscope (E600, Nikon USA), a 2 W 532 nm laser (Millennia II, Spectra Physics, Mountain View, CA), and an *f*/1.8 axial transmissive spectrograph (HoloSpec, Kaiser Optical Systems, Inc., Ann Arbor, MI). An infinity corrected 10×0.45 NA plan achromat objective (Nikon) was used for focusing the 532 nm laser line onto the specimen and for collecting the Raman scatter. The spectrograph was fitted with a 512×512 pixel back-illuminated EMCCD (iXON, Andor Technology, Belfast, Northern Ireland.) and operated at full gain was used. A uniform laser line was generated using a 5° Powell lens (StockerYale Canada, Montreal, PQ) [29]. Hyperspectral images are built up by scanning the line-focused laser across the specimen [30] using a single axis scanning mirror (6240H, Cambridge Technology, Inc., Cambridge, MA) placed between the microscope and the long-pass filter (Fig. 1). A LabVIEW (National Instruments, Austin, TX) program controls the mirror's position by adjusting the voltage sent to the mirror control board through a 12-bit digital-analog converter. The mirror could be positioned to approximately ±0.2 μm with a settling time 1–3 ms.

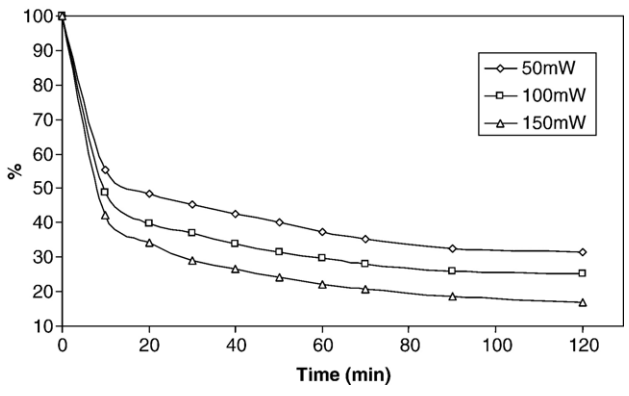

Fig. 3. Percentage decrease of background intensity at different photobleaching time for various laser powers.

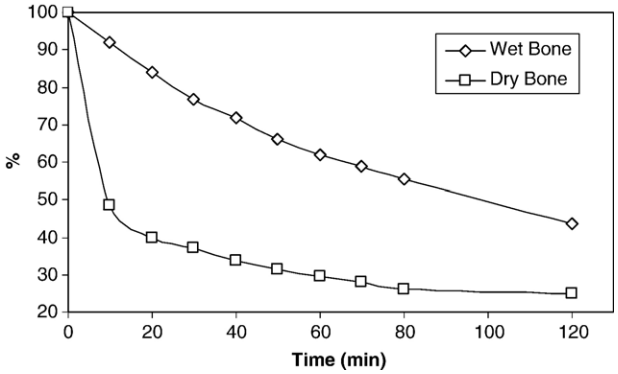

Fig. 4. Time dependence of fluorescence background reduction for wet and dry bone. Laser power is 100 mW.

The spectrograph was calibrated against an Ar emission lamp. Spectral data analysis was performed with Matlab (Math Works, Inc.) or in GRAMS/32 (Galactic Industries). Prior to data analysis, all spectral data were processed with removal of the curvature of the spectral bands due to the large gathering angle of the spectrograph, subtraction of dark current and removal of noise spikes. The spectra were analyzed using principal components analysis to identify spectral factors and band-target entropy minimization (BTEM) [31] to extract the spectra and generate score plot images.

Bovine bone specimens obtained from a local abattoir were sectioned into 5×2×10 mm blocks under constant irrigation using a diamond wheel saw (South Bay Technology, Inc., San Clemente, CA). Sections were rinsed with calcium-buffered saline (CBS) solution to remove any residues and blood. Calcium buffering is required to maintain bone stiffness in saline solution. CBS solution is comprised of 0.57% $CaCl_2$ and 1% sodium azide (as an antibiotic) in phosphate-buffered saline (Invitrogen, Carlsbad, CA) solution, buffered to pH=7.4 [32]. The rinsed sections were then wrapped in calcium saline soaked gauze, and frozen (−30 °C) until required.

Two different photobleaching protocols were examined. In protocol 1 a bone specimen was removed from CBS, allowed to dry superficially and photobleached for 10 s–5 min prior to Raman data acquisition. In protocol 2, the specimen was kept moist by suspension in a chamber with a cover containing an opening just large enough to accommodate a microscope objective [12]. High humidity was maintained by a thin layer of water in the bottom of the chamber. Just prior to an experiment, a bone specimen was briefly immersed in deionized water to establish hydration and then photobleached for 2–20 min prior to Raman data acquisition.

To measure the time dependence of the photobleaching process, each Raman spectrum was acquired using 4 s integration times at 15 min intervals over a 2-h period. To test the effect of multiple scattering (photon migration) on bleaching efficiency, specimens were prebleached for 15 min and 4 s integration spectra were obtained continuously for times of 160–180 s.

Raman imaging was performed on a section of fresh bovine cortical bone. A line focused 532 nm laser was focused onto the specimen through a Nikon 10X/0.45 NA plan apochromat objective, providing incident laser power of 100 mW. A series of 100 transects of Raman spectra spaced 1.0 μm apart (2.0 μm spatial resolution) were acquired to construct 296 μm×107 μm (H×W) image. The integration time for each transect was 4 s. The specimen was photobleached with line illumination at one end of the scanned region for approximately 15 min prior to Raman data acquisition. BTEM [31] has been applied to extraction of Raman spectra and Raman images from Raman imaging microspectroscopy data sets. Bands in non-noise eigenvectors that

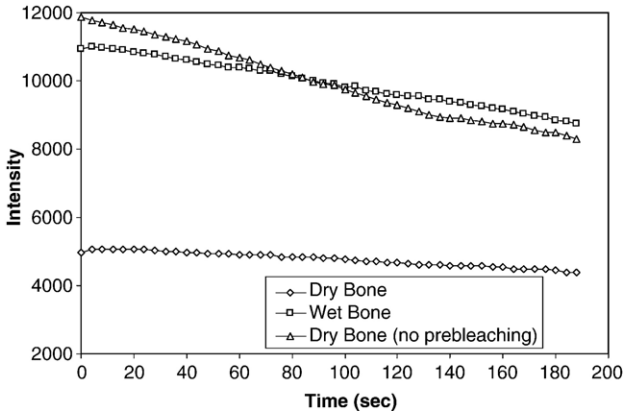

Fig. 5. The short time dependence of fluorescence background.

would normally be used for recovery of spectra are examined for localized spectral features. For a targeted (identified) band, entropy minimization is used to recover the spectrum containing this feature from the non-noise eigenvectors [33].

3. Results and discussion

It was observed that the exact time dependence of fluorescence photobleaching depended on the specimen used, the pretreatment employed and the position of the laser beam on the specimen. In general, pretreatment to remove blood reduced bleaching time and superficially dry specimens photobleached more rapidly than fully hydrated specimens. Therefore, it was necessary to establish bleaching times required for each specimen empirically before beginning an image acquisition. Representative data are presented here.

Fig. 2 shows representative Raman spectra of bone photobleached according to protocol 1 as a function laser irradiation time. At the beginning of an experiment most of the Raman bands are observed on a high fluorescence background. Fig. 3 shows a time sequence of Raman spectra of bone photobleached according to protocol 1 as a function laser power. After about 15 min, the fluorescence background is reduced to 50% or less of the initial value, depending on the total laser power. Further

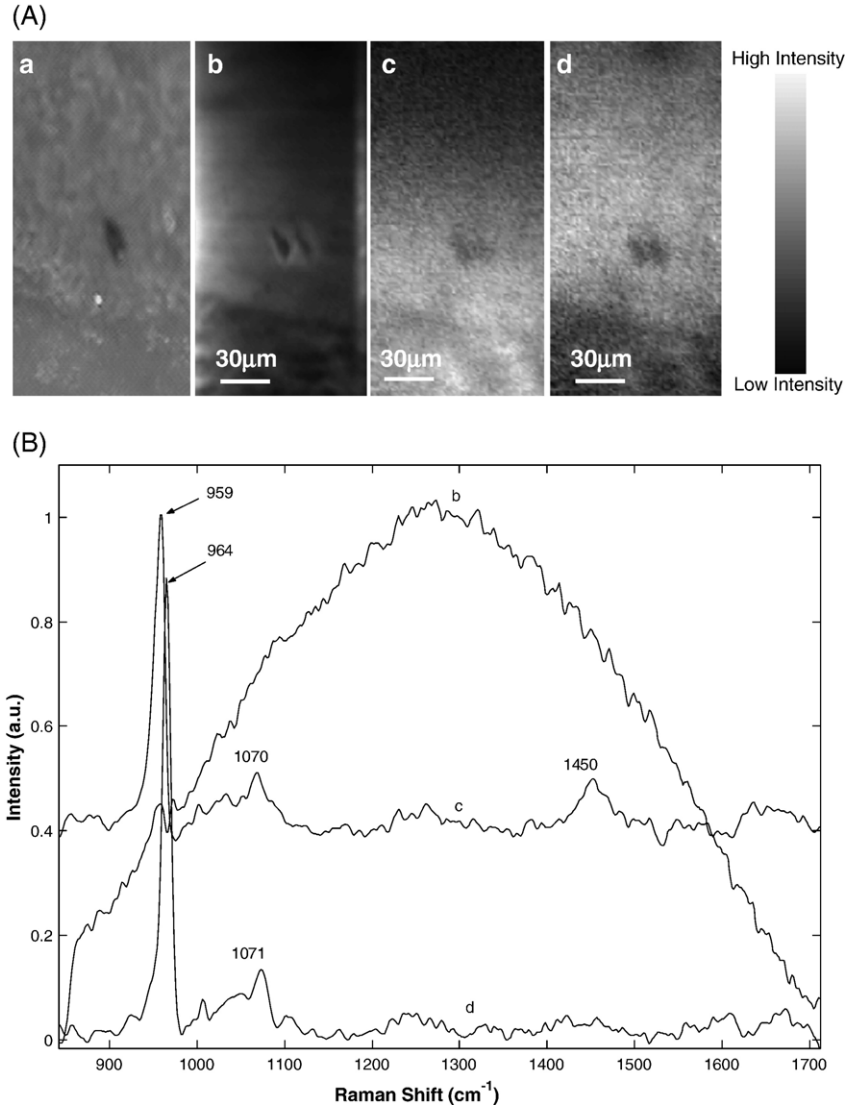

Fig. 6. (A) Reflected light (a), fluorescence (b) and Raman images (c and d) of a section of cortical bone, and (B) corresponding Raman spectra. Raman spectra corresponding to Raman images are indicated with the same lowercase letter. Raman images are 296 μm × 107 μm with 2 μm resolution.

decrease occurs over time, but the rate is much lower. The photobleaching rate is much lower if the bone is immersed in water or CBS (Fig. 4). For the specimen shown in this figure, prebleaching a superficially dry bone for about 15 min reduces the fluorescence background to about 45% of the initial value, but results in only a 15% reduction in fluorescence of tissue immersed in water or CBS.

The Raman spectrum of bone has prominent and well-characterized mineral and matrix bands in the 800–1680 cm^{-1} observation window. Phosphate ν_1 is found at 959–960 cm^{-1}. Carbonate ν_1 is found at 1069–1071 cm^{-1}. The major Raman signatures of matrix in this region are amide III at 1245–1250 cm^{-1}, CH_2 scissoring at 1447–1451 cm^{-1} and part of the largest component of amide I envelope at 1668–1672 cm^{-1}. The Raman band positions and band intensities show no significant change (<3%) throughout the 20-min photobleaching period. While we cannot demonstrate the complete absence of photochemical damage to bone matrix, most of the background reduction is due to the bleaching of other fluorophores.

However, prolonged photobleaching of dry bone (>30 min) can alter the mineral to matrix band area ratio by 4–6%. Although, the mechanism behind these changes is unclear, it is likely to involve dehydration of the matrix component as a result of laser-induced thermal heating effects. Photolysis of collagen cross-links by a 532-nm excitation is also a plausible mechanism, even though the excitation wavelength (ca. 325 nm) is well below the 532 nm irradiation wavelength used in this study. Further work is necessary to establish the rate of collagen cross-link photolysis using both visible and UV excitation wavelengths. However, Ager et al. [34] has successfully shown that UV Raman spectrum of human cortical bone can be obtained without degrading the matrix component by using low laser powers (<5 mW) and by spinning the specimen rapidly using a custom-made rotating stage (~45 rpm).

The short time dependence of fluorescence background is shown in Fig. 5. The number counts is recorded, to show that the wet bone has a higher background than the dry, and has as a slower rate of photobleaching. With about 15 min of prebleaching, the dry tissue has a low and very slowly decaying background, as shown in Fig. 5. These results are consistent with partial replenishment in the wet specimen of fluorophores in the illumination region, presumably by transport of water-soluble material, such as FAD or heme.

Fig. 6A shows reflected light (frame a), fluorescence (frame b) and Raman images (frames c and d) of a section of partially damaged cortical bone. Raman spectra corresponding to each frame are labeled with the same lowercase letter, and are shown in Fig. 6B. A 15-min prebleach was performed at the left edge of the scanned region, and the line scan direction was left to right. The features are similar in each image, except that the two mineral component Raman images show different spatial dependences (Fig. 6c and d). In the region of undamaged tissue, the phosphate ν_1 band was found at 959 cm^{-1}, as expected for the carbonated hydroxyapatic bone mineral. However, in the region of damage, the additional phosphate ν_1 band was observed at 964 cm^{-1} and interpreted as a more stoichiometric, less carbonated mineral species. The spatial locations of these two phosphate factors are important information contained in Raman images.

The surprising effect is that the fluorescence background is almost constant across the entire Raman image, even though the image is 100 scans wide. We attribute this effect to photon migration [15–21]. Although photons are injected in a line along the left side of each image, scattering causes them to diffuse across the entire field of view, and even further. The propagation time is a few tens of picoseconds and the attenuation over 100 μm is small enough that photobleaching efficiency is nearly constant. If the tissue is dry, it is not necessary to prebleach at every point to be imaged.

A similar effect is observed with bone tissue that is fixed and embedded in polymethyl methacrylate. Using murine cortical bone, we have confirmed that a 15-min prebleach is effective in reducing fluorescence background over a ~300 μm × 100 μm field of view. However, we were not able to achieve similar results with tissue that was immersed. The failure of the single line prebleach is expected because immersion allows fluorophore replenishment, negating much of the benefit of photon migration.

We conclude that photon migration can be used to reduce prebleaching time to a surprisingly short value. The methodology is not completely general, but is readily applicable to archived specimens. In view of the demonstrated importance of maintaining hydration of fresh bone in Raman biomechanical studies, single line prebleaching cannot be recommended for such applications.

Acknowledgement

This work has been supported by NIH grant R01 AR052010 to M.D.M.

References

[1] M.L. Bouxsein, Determinants of skeletal fragility, Best Pract. Res., Clin. Rheumatol. 19 (2005) 897–911.
[2] C.E. Hoffler, K.E. Moore, K. Kozloff, P.K. Zysset, M.B. Brown, S.A. Goldstein, Heterogeneity of bone lamellar-level elastic moduli, Bone 26 (2000) 603–609.
[3] K.J. Goodwin, N.A. Sharkey, Material properties of interstitial lamellae reflect local strain environments, J. Orthopaedic. Res. 20 (2002) 600–606.
[4] J.Y. Rho, P. Ziopos, J.D. Currey, G.M. Pharr, Variations in the individual thick lamellar properties within osteons by nanoindendation, Bone 25 (1999) 295–300.
[5] S. Hengsberger, P. Ammann, B. Legros, R. Rizzoli, P. Zysset, Intrinsic bone tissue properties in adult rat vertebrae: modulation by dietary protein, Bone 36 (2005) 134–141.
[6] D.B. Burr, The contribution of the organic matrix to bone's material properties, Bone 31 (2002) 8–11.
[7] R.K. Nalla, J.J. Kruzic, J.H. Kinney, R.O. Ritchie, Aspects of in vitro fatigue in human cortical bone; time and cycle dependent crack growth, Biomaterials 26 (2005) 2183–2195.
[8] J.A. Timlin, A. Carden, M.D. Morris, R.M. Rajachar, D.H. Kohn, Raman spectroscopic imaging markers for fatigue-related microdamage in bovine bone, Anal. Chem. 72 (2000) 2229–2236.
[9] M.D. Morris, A. Carden, R.M. Rajachar, D.H. Kohn, Effects of applied load on bone tissue as observed by Raman spectroscopy, Proc. SPIE 4614 (2002) 47–54.

[10] A. Carden, R.M. Rajachar, M.D. Morris, D.H. Kohn, Ultrastructural changes accompanying the mechanical deformation of bone tissue: a Raman imaging study, Calcif. Tissue Int. 72 (2003) 166–175.
[11] M.D. Morris, W.F. Finney, R.M. Rajachar, D.H. Kohn, Bone tissue ultrastructural response to elastic deformation probed by Raman spectroscopy, Faraday discuss. 126 (2004) 159–168.
[12] A.C. Callender, W.F. Finney, M.D. Morris, N.D. Sahar, D.H. Kohn, K.M. Kozloff, S.A. Goldstein, Dynamic mechanical testing system for Raman microscopy of bone tissue specimens, Vib. Spectrosc. 38 (2005) 101–105.
[13] A. Stewart, D.A. Shea, C.p. Tarnowski, M.D. Morrisd, D. Wang, R. Franceschi, D.L. Lin, E. Keller, Trends in early mineralization of murine calvarial osteoblastic cultures: a Raman microscopic study, J. Raman Spectrosc. 33 (2002) 536–543.
[14] J.R. Janesick, Scientific charge coupled devices, SPIE press, USA, 2001.
[15] P. Matousek, I.P. Clark, E.R.C. Draper, M.D. Morris, A.E. Goodship, N. Everall, M. Towrie, W.F. Finney, A.W. Parker, Subsurface probing in diffusely scattering media using spatially offset Raman spectroscopy, Appl. Spectrosc. 59 (2005) 393–400.
[16] N. Everall, T. Hahn, P. Matousek, A.W. Parker, M. Towrie, Photon migration in Raman spectroscopy, Appl. Spectrosc. 58 (2004) 591–597.
[17] N. Everall, T. Hahn, P. Matousek, A.W. Parker, M. Towrie, Picosecond time-resolved Raman spectroscopy of solids: capabilities and limitations for fluorescence rejection and the influence of diffuse reflectance, Appl. Spectrosc. 55 (2001) 1701–1708.
[18] M.D. Morris, A.E. Goodship, E.R.C. Draper, P. Matousek, M. Towrie, A.W. Parker, Kerr-gated picosecond Raman spectroscopy and Raman photon migration of equine bone tissue with 400-nm excitation, Proc. SPIE 5321 (2004) 164–169.
[19] M.D. Morris, P. Matousek, M. Towrie, A.W. Parker, A.E. Goodship, E.R.C. Draper, Kerr-gated time-resolved Raman spectroscopy of equine cortical bone tissue, J. Biomed. Opt. 10 (2005) 014014.
[20] E.R.C. Draper, M.D. Morris, N.P. Camacho, P. Matousek, M. Towrie, A.W. Parker, A.E. Goodship, Novel assessment of bone using time-resolved transcutaneous Raman spectroscopy, J. Bone Miner Res. 20 (2005) 1968–1972.
[21] M.V. Schulmerich, W.F. Finney, R.A. Fredericks, M.D. Morris, Subsurface Raman spectroscopy and mapping using a globally illuminated non-confocal fiber optic array probe in the presence of Raman photon migration, Appl. Spectrosc. 60 (2006) 109–114.
[22] C.G. Coates, D.J. Denvir, N.G. Mchale, K.D. Thornbury, M.A. Hollywood, Optimizing low-light microscopy with back-illuminated electron multiplying charge-coupled device: enhanced sensitivity, speed, and resolution, J. Biomed. Opt. 9 (2004) 1244–1252.
[23] A. Sarkar, R.B. Robertson, J.M. Fernandez, Simultaneous atomic force microscopy and fluorescence measurements of protein unfolding using a calibrated evanescent wave, Proc. Natl. Acad. Sci. 101 (2004) 12882–12886.
[24] S.V. Patwardhan, S.R. Bloch, S. Achilefu, J.P. Culver, Time-dependent whole-body fluorescence tomography of probe bio-distributions in mice, Opt. Express 13 (2005) 2564–2577.
[25] G. Penel, G. Leroy, E. Brés, New preparation method of bone samples for Raman microspectroscopy, Appl. Spectrosc. 52 (1998) 312–313.
[26] T.-C. Chen, D.A. Shea, M.D. Morris, Effect of hydrogen peroxide bleaching on bone mineral/matrix ratio, Appl. Spectrosc. 56 (2002) 1035–1037.
[27] D.A. Shea, M.D. Morris, Bone tissue fluorescence reduction for visible laser Raman spectroscopy, Appl. Spectrosc. 56 (2002) 182–186.
[28] K.A. Christensen, M.D. Morris, Hyperspectral Raman microscopic imaging using Powell lens line illumination, Appl. Spectrosc. 52 (1998) 1145–1147.
[29] A. Bewsher, I. Powell, W. Boland, Design of single element laser beam shape projectors, Appl. Opt. 35 (1996) 1654–1958.
[30] P.J. Treado, M.D. Morris, Infrared and Raman spectroscopic imaging, in: M.D. Morris (Ed.), Spectroscopic imaging of the chemical state, Dekker, New York, 1993.
[31] E. Widjaja, N. Crane, TC. Chen, M.D. Morris, M.A. Ignelzi, B.R. McCreadie, Band-Target Entropy Minimization (BTEM) Applied to Hyperspectral Raman Image Data, Appl. Spectrosc. 57 (2003) 1353–1362.
[32] M.B. Gustafson, R.B. Martin, V. Gibson, D.H. Storms, S.M. Stover, J. Gibeling, L. Griffin, Calcium buffering is required to maintain bone stiffness in saline solution, J. Biomech. 29 (1996) 1191–1194.
[33] N.J. Crane, M.D. Morris, M.A. Ignelzi, G. Yu, Raman imaging demonstrates FGF2-induced craniosynostosis in mouse calvaria, J. Biomed. Opt. 10 (2005) 031119–031128.
[34] J.W. Ager III, R.K. Nalla, K.L. Breeden, R.O. Ritchie, Deep-ultraviolet Raman spectroscopy study of the effect of aging on human cortical bone, J. Biomed. Opt. 10 (2005) 034012–034018.